The Kuroshio nutrient stream and its temporal variation in the East China Sea

Xinyu Guo,[1,2] Xiao-Hua Zhu,[2,3] Qing-Song Wu,[2] and Daji Huang[2,3]

Received 14 May 2011; revised 10 November 2011; accepted 21 November 2011; published 31 January 2012.

[1] Using in situ data from 88 cruises from 1987 to 2009 in the East China Sea, downstream nutrient flux (the product of velocity and nutrient concentration) and nutrient transport (integration of flux over a section) by Kuroshio were examined. The presence of a maximum nutrient flux core in the middle layer was confirmed. Seasonal variation in the nutrient flux was not significant and was much smaller than interannual variations. The change in the Kuroshio speed and current structure were major causes for interannual variations in the nutrient flux. The downstream nitrate transport by the Kuroshio in the East China Sea had a mean value of 170.8 kmol s^{-1} and a standard deviation of 41.6 kmol s^{-1}. The mean seasonal nitrate transport ranged between about 161 and 177 kmol s^{-1} and the absolute interannual variation from about 100 to 280 kmol s^{-1}. The phosphate flux and phosphate transport can be approximately estimated by the ratio (13.64) of nitrate concentration to phosphate concentration. The nitrate concentration in the middle and bottom layers across the Kuroshio in the East China Sea was found to increase significantly over the 23 year period, and especially after 2004 but not at ratios with oxygen that suggest increased remineralization of organic matter. The nutrient transport, however, did not increase significantly because increases in the surface layer were offset by decreases in the middle and bottom layers caused by reduction in velocity in the density ranges of 26.0 to 27.2 σ_θ below the Kuroshio.

Citation: Guo, X., X.-H. Zhu, Q.-S. Wu, and D. Huang (2012), The Kuroshio nutrient stream and its temporal variation in the East China Sea, *J. Geophys. Res.*, *117*, C01026, doi:10.1029/2011JC007292.

1. Introduction

[2] The idea of a nutrient stream that transports nutrients along a west boundary current has been proposed for the Gulf Stream for many years [*Pelegrí and Csanady*, 1991; *Pelegrí et al.*, 1996]. The Gulf Stream's counterpart in the North Pacific, the Kuroshio, is naturally expected to have the same function as the Gulf Stream for transporting nutrients along it, from its origin area, east of Luzon Island where it forms as a northward branch of the westward North Equatorial Current, to the Kuroshio Extension (Figure 1a). *Robbins and Bryden* [1994] estimated the meridional nutrient transport in the North Pacific Ocean but did not pay special attention to the role of Kuroshio. *Chen et al.* [1994, 1995a] first reported nutrient flux and nutrient transport by the Kuroshio based on four cruises along a section extending eastward from Taiwan.

[3] The nutrient stream results from the strong western boundary current and the high nutrient concentration within the water that is carried by this boundary current. As a result of reduced current speed and increased nutrient concentration with depth, the nutrient flux, defined as the product of the current speed and nutrient concentration, usually has a subsurface high value. The current, which is faster at its center than at its sides, further produces a subsurface core with a maximum nutrient flux [*Pelegrí and Csanady*, 1991].

[4] Our first objective in this study is to present the vertical structure of mean nutrient flux based on long-term repeat observations across the Kuroshio in the East China Sea. On one hand, the vertical gradients of current speed and nutrient concentration in the Kuroshio region are probably different from those in the Gulf Stream; the comparison of nutrient flux in two western boundary currents is therefore an interesting issue. On the other hand, reports by *Chen et al.* [1994, 1995a] were based on four cruises across the Kuroshio and their results may be affected by some processes with short time scales, e.g., the passage of mesoscale eddies. By averaging long-term repeated observations, we expect to present a robust document on the mean state of nutrient flux by the Kuroshio in the East China Sea.

[5] Our second purpose in this study is to examine the temporal variations in nutrient flux and nutrient transport by the Kuroshio in the East China Sea. It has been demonstrated that the nutrients carried by the Gulf Stream can reach the euphotic layer and contribute to the primary production in

[1]Center for Marine Environmental Studies, Ehime University, Matsuyama, Japan.
[2]State Key Laboratory of Satellite Ocean Environment Dynamics, Second Institute of Oceanography, State Oceanic Administration, Hangzhou, China.
[3]Department of Ocean Science and Engineering, Zhejiang University, Hangzhou, China.

0148-0227/12/2011JC007292

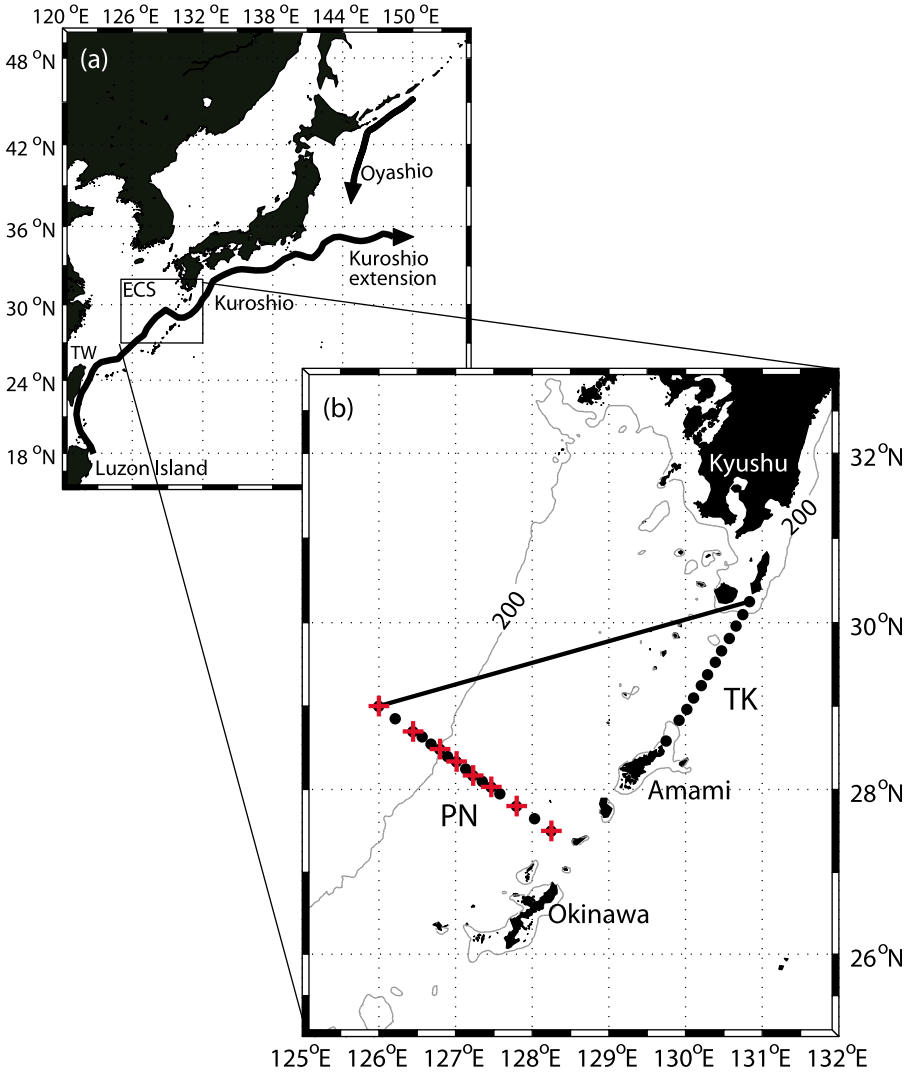

Figure 1. (a) Study area and schematic image of Kuroshio path. ECS denotes East China Sea; TW denotes Taiwan. (b) Position of hydrographic stations for water temperature and salinity (black dots) and for nutrient concentrations (red plus signs). Line marked "200" denotes 200 m isobath.

the North Atlantic [*Pelegrí et al.*, 2006; *Williams et al.*, 2006]. In the North Pacific, high primary production has been reported in the Kuroshio/Oyashio mixing region [e.g., *Tadokoro et al.*, 2009]. Since the nutrient concentration is higher in the Oyashio water than in the Kuroshio water, the nutrients carried by the Oyashio from subpolar region to this region likely contribute mostly to the high primary production there. However, the mixing nature of two water masses indicates that the nutrients carried by the Kuroshio may also contribute to the primary production in this region and will have an impact in all waters being influenced by the subarctic current across the Pacific. For this reason, a good documentation of the temporal variations in nutrient flux and nutrient transport by the Kuroshio will add new material for understanding the long-term variations in the nutrients and primary production in the Kuroshio/Oyashio mixing region.

[6] In the long journey from its origin to the Kuroshio Extension area, the Kuroshio has a relatively more stable path along the shelf break of the East China Sea than in other regions. This provides good conditions for monitoring its temporal variations. In fact, the Japan Meteorological Agency has maintained a section across the Kuroshio in the East China Sea for more than 40 years. Using the hydrographical and nutrient data from such long-term observations, we examined the spatial structure of nutrient flux and the temporal variations of nutrient flux and nutrient transport by the Kuroshio in the East China Sea.

[7] In section 2, we give a brief description of the observations and the data processing procedures, such as the inverse method being used to calculate the velocity normal to the section from hydrographic data, and the linear interpolation of nutrient data to the velocity grid points. In section 3, we present the spatial distribution of mean nutrient flux and examine temporal variations in the nutrient flux by using empirical orthogonal function (EOF) analysis and by directly decomposing the variance of nutrient flux into several terms that depend on the variances of velocity and nutrient concentration. The temporal variations of nutrient transport, with attention to the differences before 2004 and after 2004, are also given in section 3. In section 4, we give

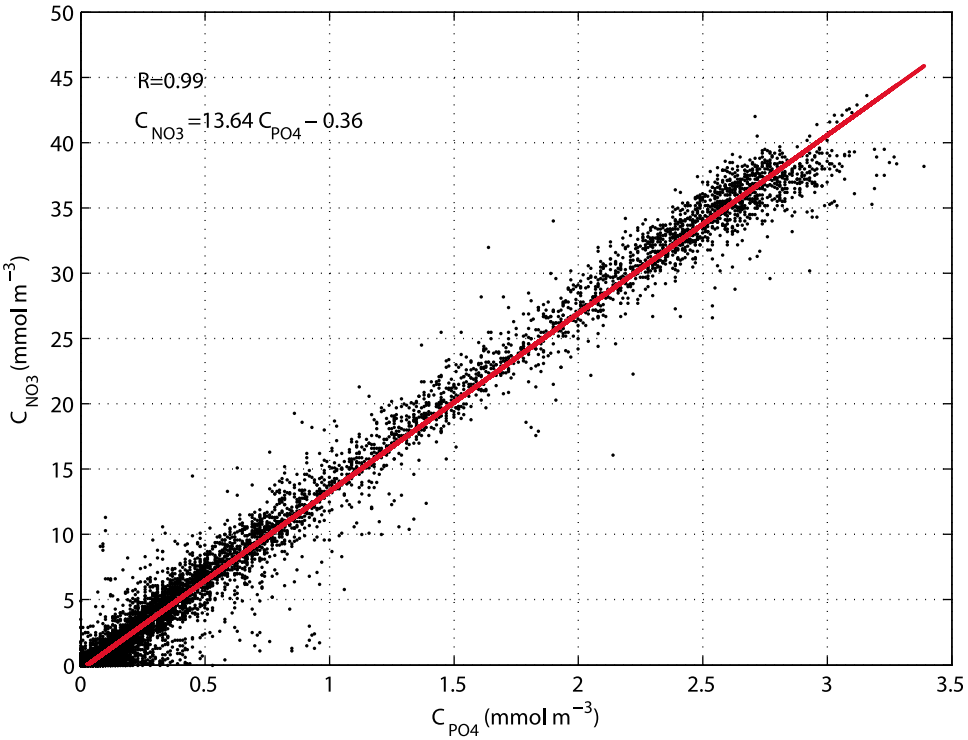

Figure 2. Scatterplot of nitrate concentration (C_{NO3}) versus phosphate concentration (C_{PO4}). The correlation coefficient between C_{NO3} and C_{PO4} is 0.99. The linear regression of C_{NO3} to C_{PO4} gives a ratio of 13.64 and a cutoff of -0.36 mmol m^{-3} of C_{NO3}.

an analysis on possible causes for the differences in velocity and nutrient concentrations before 2004 and after 2004 and compare spatial structures of nutrient flux with those presented by *Chen et al.* [1994, 1995a] and those reported in the Gulf Stream region [*Pelegrí and Csanady*, 1991]. A brief summary is given in section 5.

2. Data and Processing Methods

[8] Hydrographic, nutrient, and dissolved oxygen data along two sections (PN and TK) in the East China Sea (Figure 1b) from 1965 to 2009 were obtained from Japan Meteorological Agency Web site (http://www.data.kishou.go.jp/kaiyou/db/vessel_obs/data-report/html/ship/ship.php). Since the data before 1987 were not sufficient for calculating nutrient flux, we used only the data from the 88 cruises after 1987 in this study. The hydrographic data were collected by CTD (conductivity-temperature-depth profiler); the nutrient and dissolved oxygen data were from water samples collected at standard depths and analyzed using routine methods (see *Aoyama et al.* [2008, Table 1] for analysis method details).

[9] Usually, there were four cruises every year and each cruise roughly corresponded to one season. The seasonal mean was obtained by averaging all the data from March to May for spring, from June to August for summer, from September to November for autumn, and from December to February for winter. To obtain a time series with even time intervals for the EOF analysis, we defined four fixed dates in each year (0.25, 0.50, 0.75, and 1.00) and obtained the value at a date by linearly interpolating the data before and after the given date.

[10] Hydrographic data along both section PN and section TK were used in the inverse calculation of the velocities. The inverse method [*Wunsch*, 1978] was applied to the area enclosed by section PN, section TK, and the line connecting two north stations of the sections (Figure 1b). The water exchange through two gaps between the islands at the southwestward extension of section TK was neglected. Following *Zhu et al.* [2006], the water column was vertically separated into five layers by sea surface, four isopycnals (24.5, 26.0, 26.5, and 27.2 σ_θ), and sea bottom. Mass conservation was assumed within each of five layers, while salt conservation was assumed within the lower four layers. With these conditions, the velocities at the reference level, which was set as the depth of deepest hydrographic data between each pair of stations, were obtained [*Zhu et al.*, 2006]. Applying the thermal winds relation to a pair of hydrographic stations, we then obtained the velocity normal to the line connecting two stations at 1 m interval in the vertical.

[11] The reference velocity is different for each cruise. The mean value calculated from 88 cruises at section PN varies from -0.05 to -0.1 m s^{-1} for stations west of 127°E and approaches to 0 m s^{-1} for stations east of 127°E (see bottom velocity in Figure 3b). The standard deviation is around 0.1 m s^{-1} for stations west of 127°E and decreases to 0.02 m s^{-1} for stations east of 127°E along section PN.

[12] Only data along section PN were used to calculate the nutrient flux because section TK was not sufficiently sampled. The nutrients in the Japan Meteorological Agency data set have nitrate and phosphate but not silicate. Since nitrate and phosphate concentrations have a good correlation (Figure 2), we will mainly present the results of nitrate in this study and describe those of phosphate if necessary. The

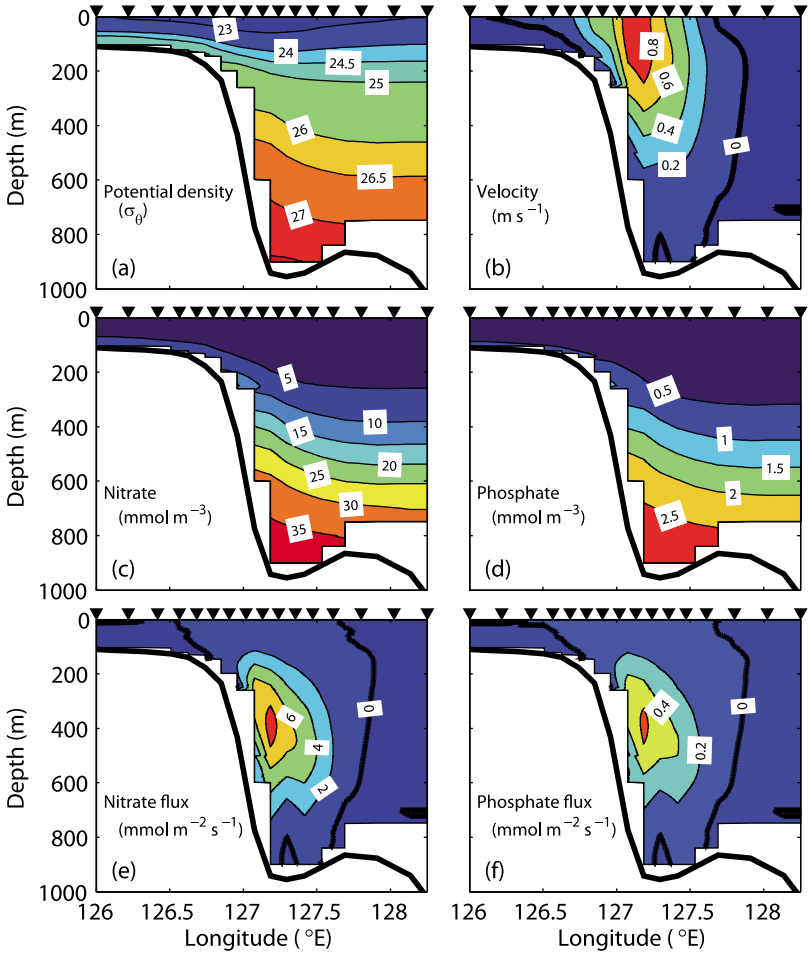

Figure 3. Average values from 88 cruises along section PN. (a) Potential density (σ_θ). (b) Velocity (m s^{-1}). (c) Nitrate concentration (mmol m^{-3}). (d) Phosphate concentration (mmol m^{-3}). (e) Nitrate flux (mmol m^{-2} s^{-1}). (f) Phosphate flux (mmol m^{-2} s^{-1}). The inverse triangles denote hydrographic stations where water temperature, salinity, and nutrient concentrations are available.

nitrate and phosphate concentrations at standard levels were first linearly interpolated to depth at one meter intervals at the hydrographic stations along section PN (Figure 1b). For calculating nutrient flux, the nutrient concentration was linearly interpolated horizontally to the grid points where current speed was determined at the same depth, and which were defined at the middle of two hydrographical stations. The nutrient transport was obtained by integrating the nutrient flux over the section.

[13] In addition to water temperature, salinity, and nutrient data, the dissolved oxygen data were used to discuss the possible causes for the temporal variations of water property in the middle and bottom layers in section 4.

3. Results

3.1. Spatial Structure of Mean Nutrient Flux

[14] The mean density, current speed, nitrate concentration, phosphate concentration, nitrate flux, and phosphate flux at section PN (Figure 3) were obtained by averaging 88 data sets from 1987 to 2009. The Kuroshio axis having maximum surface current speed can be identified over the slope (Figure 3b). The current speed decreases from the Kuroshio axis to its two sides and to the lower layer. As expected, vertical and horizontal variations in current speed are similar to the geostrophic velocity calculated with a no-motion level at 700 dbar [*Oka and Kawabe*, 1998; *Guo et al.*, 2003, Figure 9]. The total volume transport given by the current speed in Figure 3b is 22.5 Sv (1 Sv = 10^6 m^3 s^{-1}), which is close to the traditional estimate of the volume transport trough section PN [e.g., *Hinata*, 1996].

[15] The nitrate (Figure 3c) and phosphate concentrations (Figure 3d) generally increase with depth but the rate depends on water depth. The increasing rate of nutrient concentration with depth is lowest from the sea surface to ~200 m depth, is highest from ~200 m depth to ~700 m depth (e.g., ~5 mmol m^{-3} per 100 m for nitrate), and has an intermediate value from ~700 m depth to sea bottom (>900 m). The product of nitrate or phosphate concentration with current speed gives a maximum nutrient flux at ~400 m depth. There, the nitrate flux reaches 8 mmol m^{-2} s^{-1} as a product of ~20 mmol m^{-3} of nitrate concentration and 0.4 m s^{-1} of current speed, and the phosphate flux reaches 0.6 mmol m^{-2} s^{-1} as a product of ~1.5 mmol m^{-3} of phosphate concentration and 0.4 m s^{-1} of current speed.

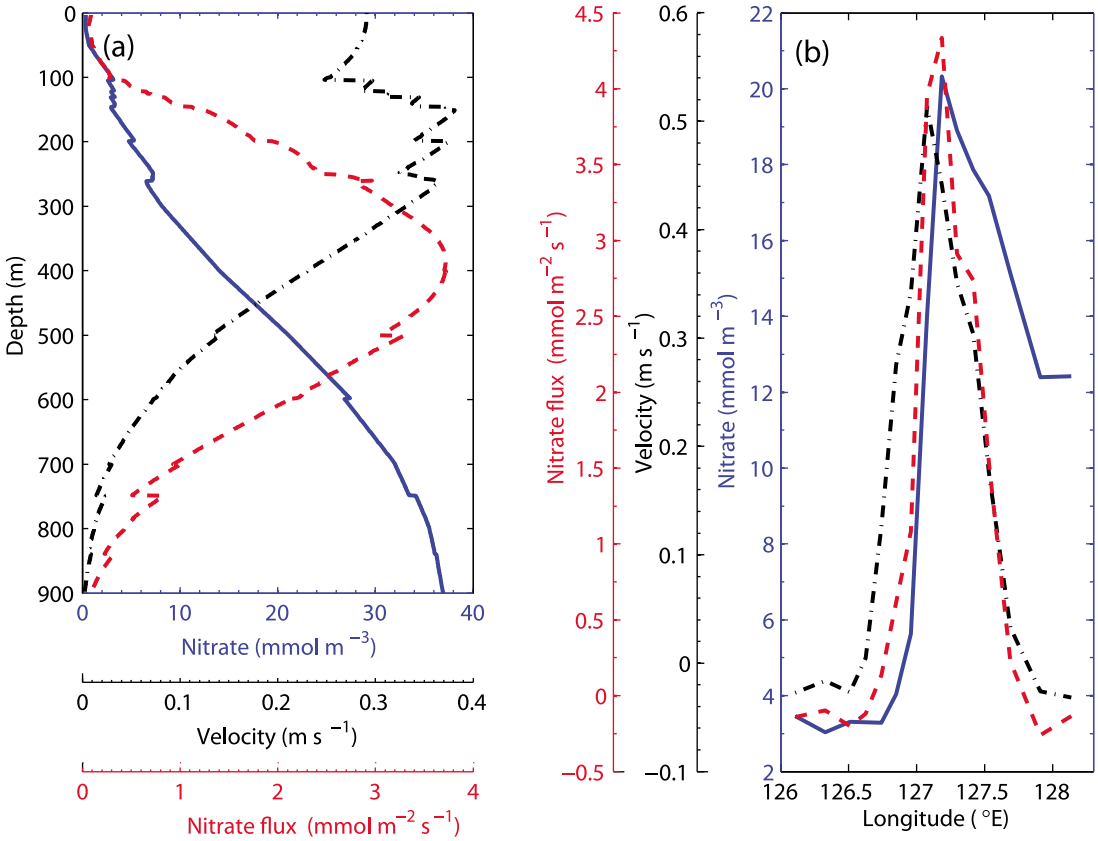

Figure 4. (a) Horizontally averaged velocity (m s^{-1}), nitrate concentration (mmol m^{-3}), and nitrate flux (mmol m^{-2} s^{-1}) along section PN. (b) Vertically averaged velocity (m s^{-1}), nitrate concentration (mmol m^{-3}), and nitrate flux (mmol m^{-2} s^{-1}) from sea bottom to sea surface.

[16] To identify the geographical position where the nutrient flux is large, the nutrient flux was averaged horizontally or vertically (Figure 4). The vertical profile of horizontally averaged nutrient flux (Figure 4a) gives a maximum value at 400 m depth and shows a reduction of nearly the same rate toward both sea surface and sea bottom. Such a profile is reasonable if we observe the vertical profile of horizontally averaged velocity and that of nutrient concentration in the same figure (Figure 4a). Horizontally, the maximum nutrient flux approximately coincides with the strongest vertically averaged velocity and the largest vertically averaged nutrient concentration (Figure 4b).

[17] To associate nutrient flux with water mass, we calculated volume and nutrient transports per unit width through five isopycnal layers (Figures 5a and 5b). The lightest layer, with density less than 24.5 σ_θ, has the largest volume transport but a small nutrient transport; the heaviest layer, with density larger than 27.2 σ_θ, has little volume transport and nutrient transport; the three layers with middle density (24.5–27.2 σ_θ) have different volume transports but very similar nutrient transports. Apparently, the nutrient transport is mainly from the three layers with middle density (24.5–27.2 σ_θ). The maximum nutrient flux is located at 26 σ_θ (Figure 5c). When plotting the nutrient flux, potential temperature, and salinity on a T-S diagram (Figure 6), the waters with relatively large nutrient flux are distributed roughly along a line connected by two water masses, the Kuroshio Intermediate Water and the Kuroshio Tropical Water (see *Chen et al.* [1995b, Table 1] for definition of two water masses). This suggests the important role of mixing between two water masses in the formation of the water with a large nutrient flux. Apparently, the Kuroshio Intermediate Water (IW) contributes more than the Kuroshio Tropical Water (TW) to the water with a large nutrient flux. Since the Kuroshio Intermediate Water has close relation to the North Pacific Intermediate Water (NPIW), we will discuss the connection between the NPIW and the water property changes at section PN in section 4.

3.2. Temporal Variations of Nutrient Flux

[18] The seasonal variation in nutrient flux is small (Figure 7). The position of the maximum nitrate flux core stays at ~400 m throughout the year. The areas with positive nutrient flux are slightly larger in winter and smaller in autumn, while the area with the nitrate flux larger than 8 mmol m^{-2} s^{-1} is slightly larger in winter and smaller in summer.

[19] An EOF analysis was applied to nitrate concentration, velocity, and nitrate flux (Figure 8). The first five EOF modes explains 47.5%, 10.6%, 10.2%, 5.2%, 4.4% of the total variance in nitrate concentration, respectively; 20.0%, 14.6%, 13.8%, 9.5%, 7.1% of the total variance in velocity, respectively; and 21.7%, 16.4%, 10.5%, 9.4%, 5.8% of the total variance in nitrate flux. The sum of first EOF mode

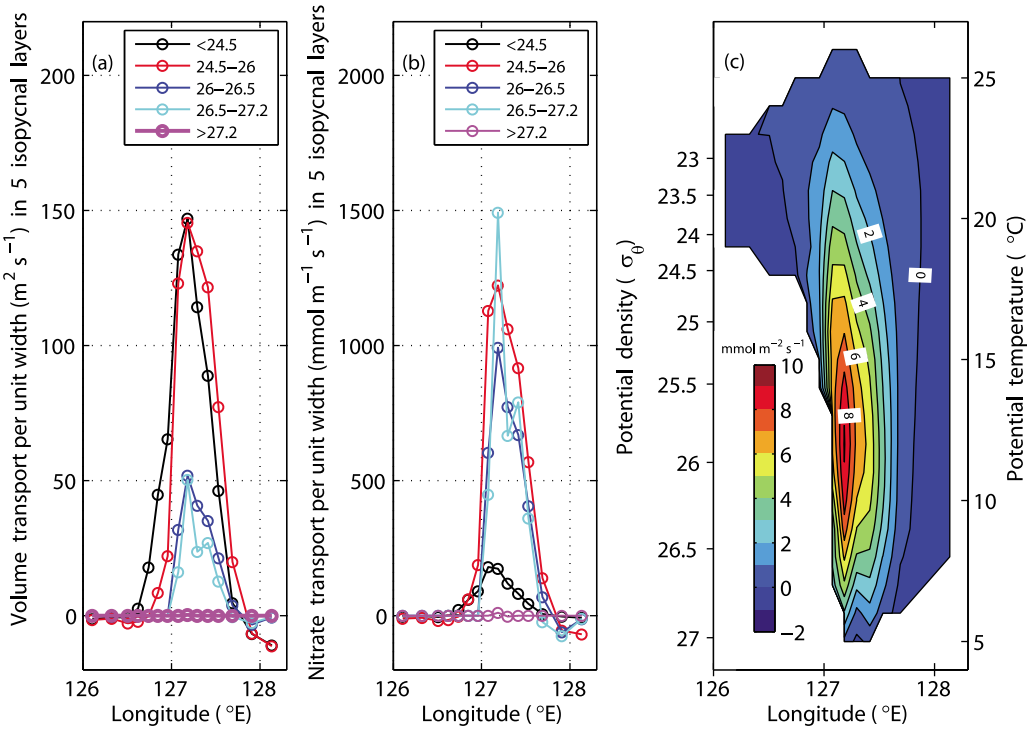

Figure 5. (a) Vertically integrated velocity (= volume transport per unit width, m^2 s^{-1}) within five isopycnal layers. (b) Vertically integrated nitrate flux (= nitrate transport per unit width, mmol m^{-1} s^{-1}) within five isopycnal layers. Circles in Figures 5a and 5b denote data grid points. (c) Distribution of nitrate flux (mmol m^{-2} s^{-1}) as a function of potential density and longitude. The potential temperature is given on the right ordinate as a reference.

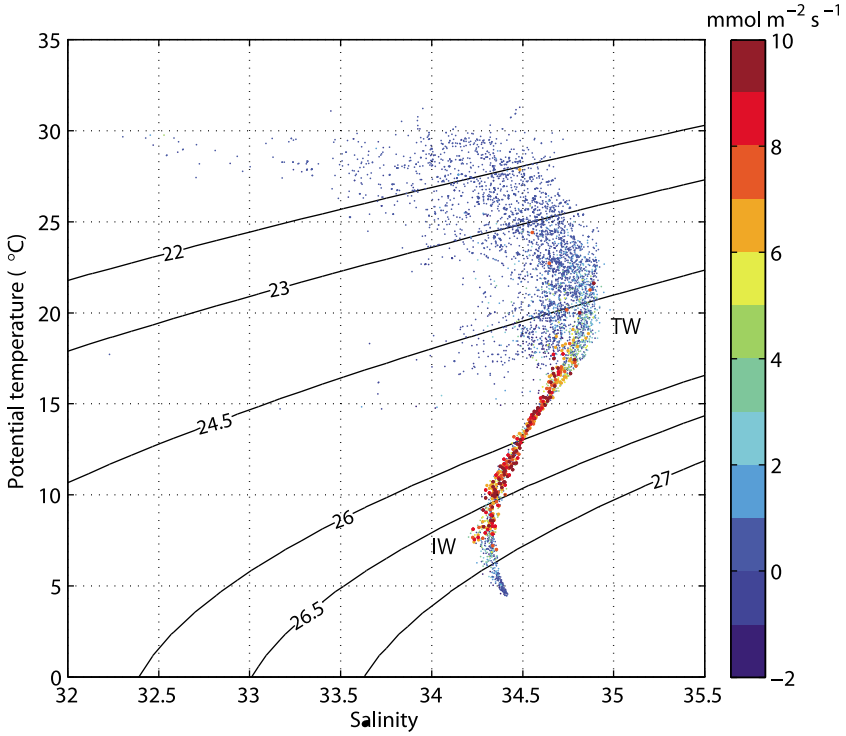

Figure 6. Nitrate flux (mmol m^{-2} s^{-1}) distribution in a T-S diagram. Colors denote nitrate flux. The contour lines with number denote potential density. TW denotes the Kuroshio Tropical Water, while IW denotes the Kuroshio Intermediate Water defined by *Chen et al.* [1995b].

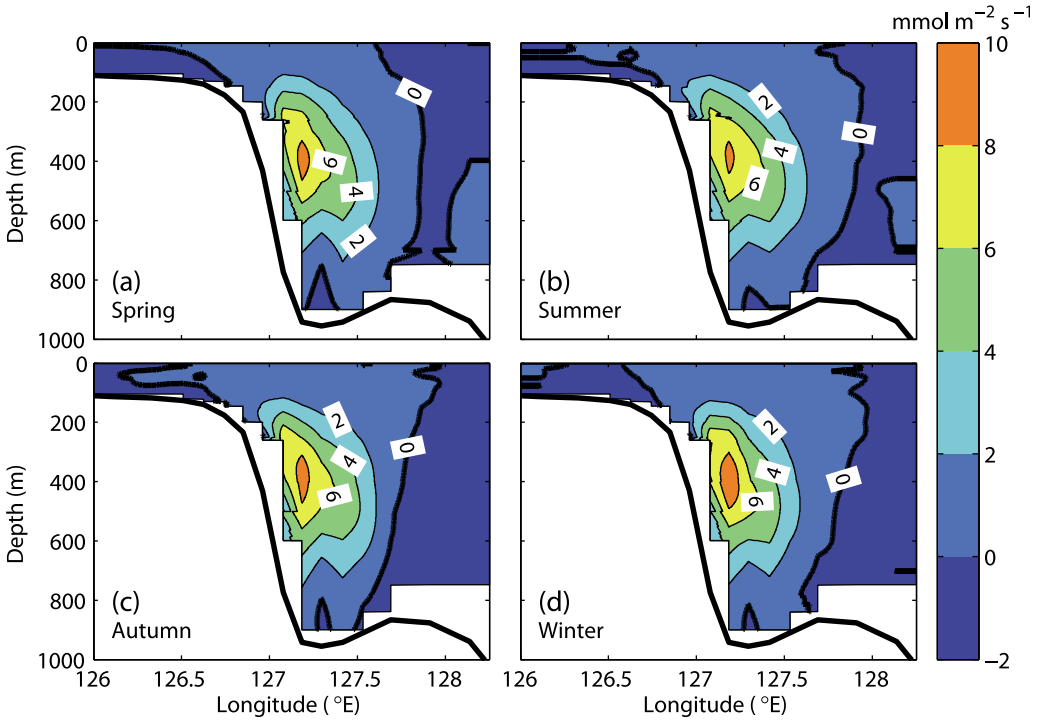

Figure 7. Average nitrate flux (mmol m^{-2} s^{-1}) in four seasons. See section 2 for definition of each season.

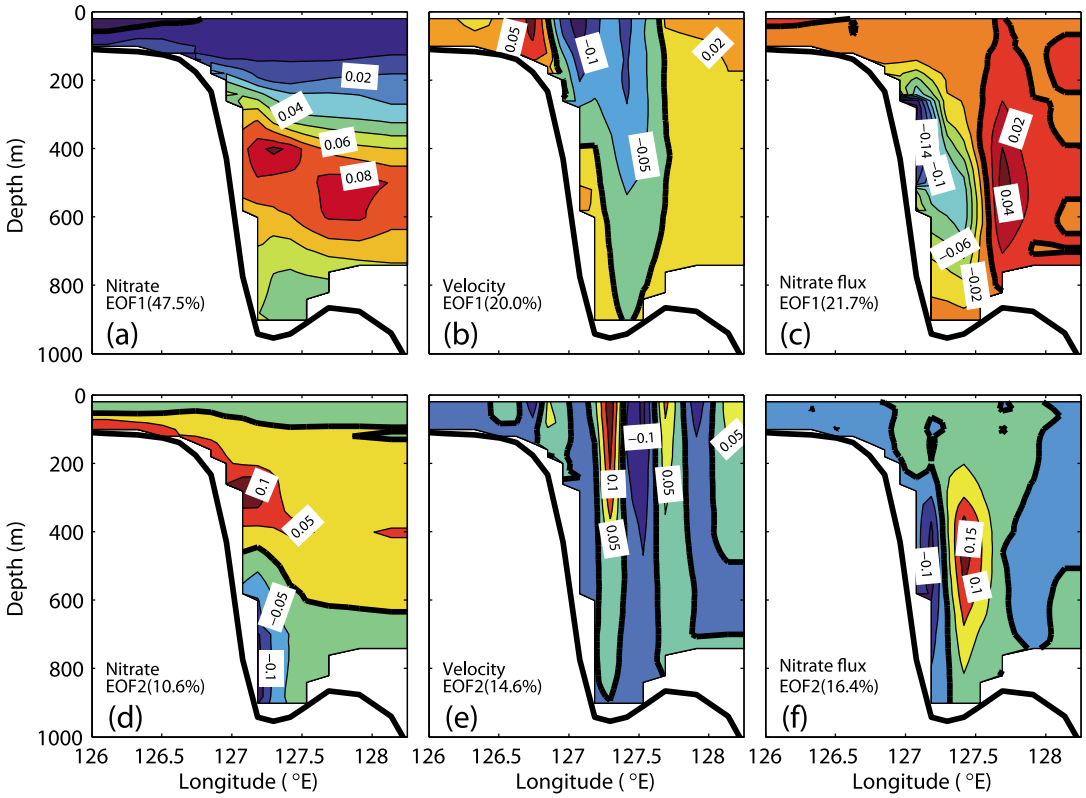

Figure 8. The first empirical orthogonal function (EOF) of (a) nitrate concentration, (b) velocity, and (c) nitrate flux. The second EOF of (d) nitrate concentration, (e) velocity, and (f) nitrate flux. The units of Figures 8a and 8d are mmol m^{-3}, those of Figures 8b and 8e are m s^{-1}, and those of Figures 8c and 8f are mmol m^{-2} s^{-1}. The numbers in brackets denote the percentage of variance explained by the corresponding EOF mode.

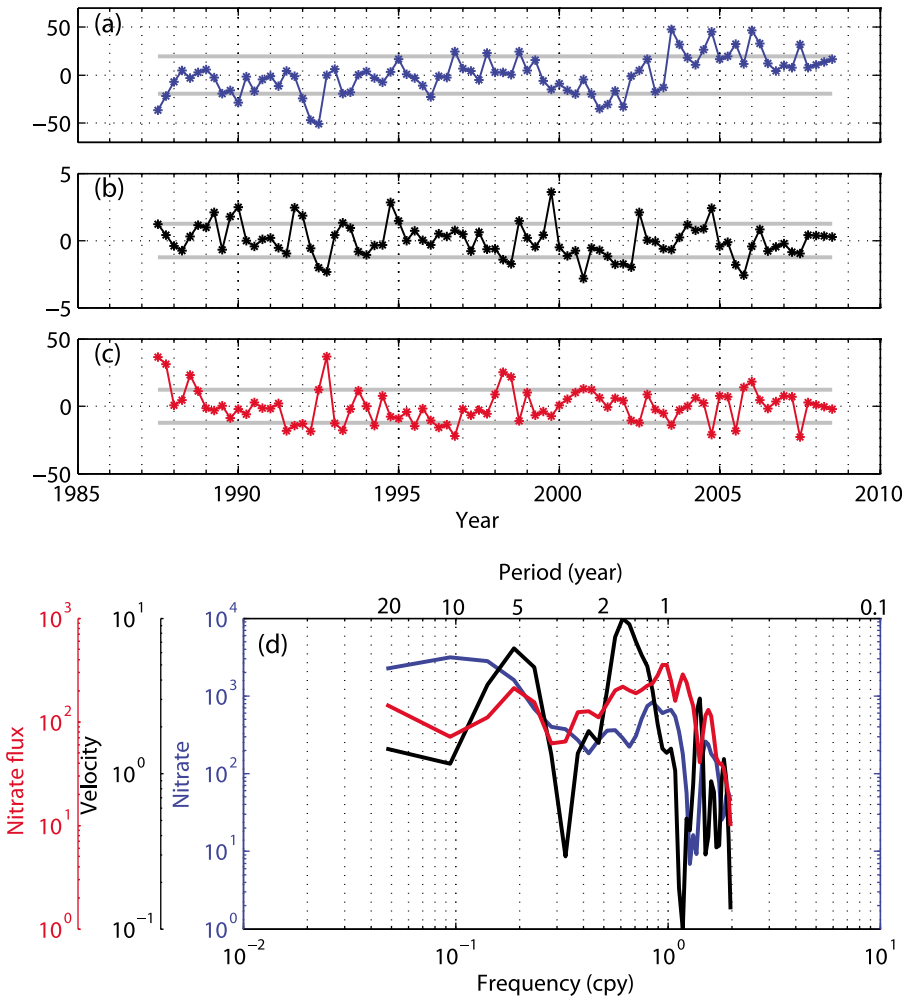

Figure 9. The time series of the first EOF principal component of (a) nitrate concentration, (b) velocity, and (c) nitrate flux and (d) their power spectral density (cpy = cycles per year). The two lines in Figures 9a–9c show mean plus and minus one standard deviation. The units in Figures 9a–9c are nondimensional.

(EOF1) and second EOF mode (EOF2) can explain more than half variability of nitrate concentration and ~40% variability of velocity and nitrate flux. The relatively low percentage explained by EOF1 and EOF2 indicate the complex temporal variations in the velocity field of this region.

[20] The EOF1 spatial pattern suggests an in-phase temporal variation in the nitrate concentration (Figure 8a) and a horizontally reversed temporal variation in the velocity (Figure 8b) and the nitrate flux (Figure 8c) over the section. The largest variances are between 400 and 600 m depth for the nitrate concentration, in the surface layer for the velocity, and around 400 m depth for the nitrate flux. The time series of the EOF1 principal component suggest that the nitrate flux (Figure 9c) has temporal variations more similar to those of velocity (Figure 9b) than to those of the nitrate concentration (Figure 9a). A period of 5 years is found in the power spectral density of the EOF1 principal component of velocity and nitrate flux (Figure 9d).

[21] To understand the mechanism responsible for the EOF1, we made a composite map of nitrate concentration, velocity, and nitrate flux (Figure 10) calculated from the cruises when the EOF1 principal component of nitrate flux is above the mean plus one standard deviation (Figure 9c), and from the cruises when the EOF1 principal component of nitrate flux is below the mean minus one standard deviation (Figure 9c), respectively. According to Figure 10, the high nitrate flux (Figure 10c) is accompanied by strong velocity (Figure 10b) while the low nitrate flux (Figure 10f) is accompanied by weak velocity (Figure 10e). The nitrate concentration has no apparent difference between these two cases (Figures 10a and 10d). The section-averaged nitrate concentration is 10.2 mmol m^{-3} for Figure 10a and 10.3 mmol m^{-3} for Figure 10d; the volume transport is 22.4 Sv for Figure 10b and 19.4 Sv for Figure 10e; the nitrate transport is 188.6 kmol s^{-1} for Figure 10c and 151.2 kmol s^{-1} for Figure 10f. All these results indicate that the EOF1 of nitrate flux can be attributed to the change in the Kuroshio speed.

[22] The EOF2 spatial pattern suggests a vertically reversed temporal variation in the nitrate concentration (Figure 8d), a horizontally fine structure of temporal variation in the velocity (Figure 8e), and a horizontally reversed temporal variation in the nitrate flux (Figure 8f). Although

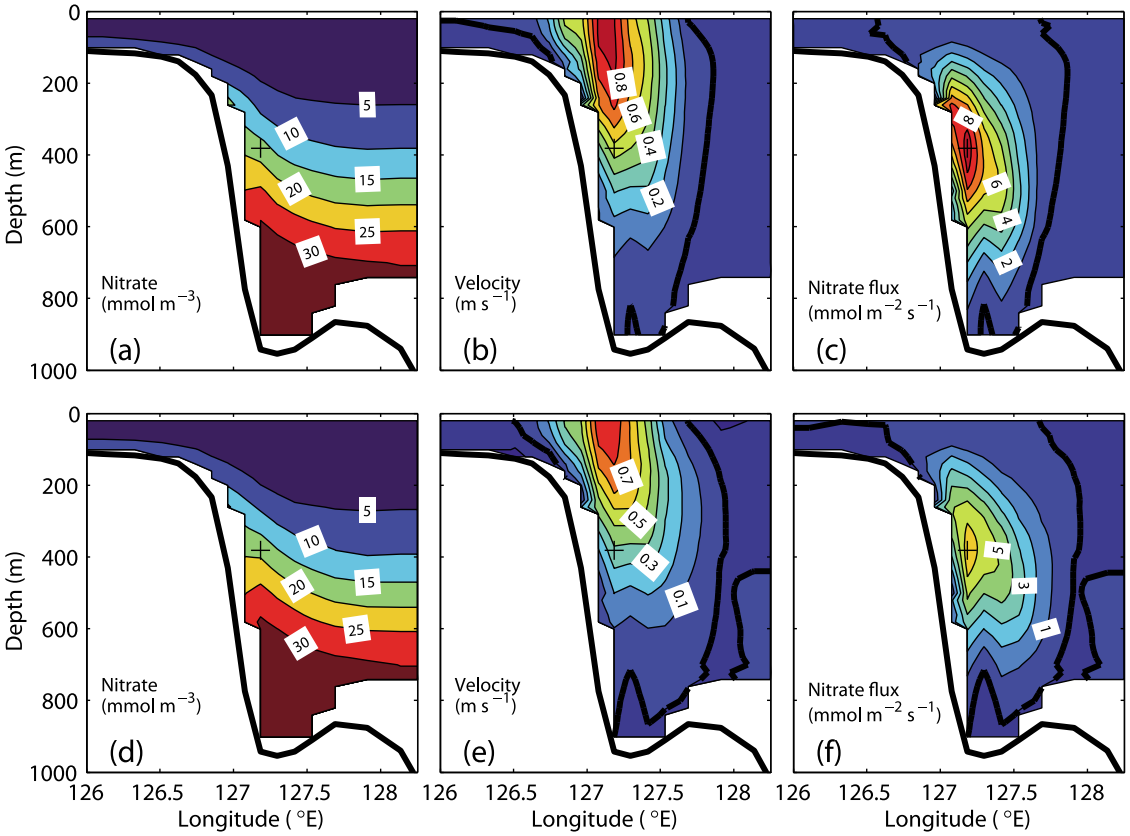

Figure 10. Composite of (a) nitrate concentration, (b) velocity, and (c) nitrate flux for the period when the first EOF principal component of nitrate flux was larger than mean plus one standard deviation. Composite of (d) nitrate concentration, (e) velocity, and (f) nitrate flux for the period when the first EOF principal component of nitrate flux was smaller than mean minus one standard deviation. The plus symbol in each plot indicates the position of maximum nitrate flux in Figure 10c or 10f.

we can observe a horizontally reversed structure in both EOF1 and EOF2 of nitrate flux, the magnitudes of positive and negative values are of different orders in the EOF1 pattern (Figure 8c) but of the same order in the EOF2 pattern (Figure 8f). The time series of the EOF2 principal component of nitrate concentration, velocity, and nitrate flux do not have a good correspondence between any two of three variables (Figures 11a–11c). A period of 1.25 year appears in the power spectral density of the EOF2 principal component of velocity and nitrate flux (Figure 11d).

[23] Following the same method as Figure 10 for EOF1, we made a composite map of nitrate concentration, velocity, and nitrate flux for the EOF2 (Figure 12). Again, the nitrate concentration does not show a significant difference at the times with high and low EOF2 principal components, respectively (Figures 12a and 12d). The section-averaged nitrate concentration is 10.2 mmol m^{-3} for Figure 12a and 10.5 mmol m^{-3} for Figure 12d. However, the difference in the nitrate flux is apparent. The differences in the maximum values and in horizontal structure of the nitrate flux can be identified in Figure 12c and Figure 12f. These differences are associated with the change in current structure, i.e., the Kuroshio became wide during the period with a high EOF2 principal component for nitrate flux (Figure 12b) while became narrow during the period with a low EOF2 principal component for nitrate flux (Figure 12e). The volume transport is 22.1 Sv for Figure 12b and 20.2 Sv for Figure 12e, while the nitrate transport is 184.0 kmol s^{-1} for Figure 12c and 166.6 kmol s^{-1} for Figure 12f.

3.3. Factors Affecting the Temporal Variance of Nutrient Flux

[24] Based on the EOF analysis, we expected that the temporal change in velocity would determine most temporal changes in the nutrient flux. To confirm this idea, we directly decomposed the variance of nutrient flux into 6 terms that can be easily explained.

[25] The velocity (V_i) and nutrient concentration (C_i) from a cruise can be expressed as sum of the mean values ($\bar{V}$, $\bar{C}$) over entire analysis period (1987–2009) and the anomalies (V_i', C_i'). Here

$$\bar{C} = \frac{1}{N}\sum_{i=1}^{N} C_i, \bar{V} = \frac{1}{N}\sum_{i=1}^{N} V_i, C_i' = C_i - \bar{C}, V_i' = V_i - \bar{V},$$

in which N is total data number and i is time index for the data. The nutrient flux ($F_i = V_i C_i$) can be then expressed as:

$$F_i = \bar{V}\bar{C} + \bar{V}C_i' + V_i'\bar{C} + V_i'C_i'. \quad (1)$$

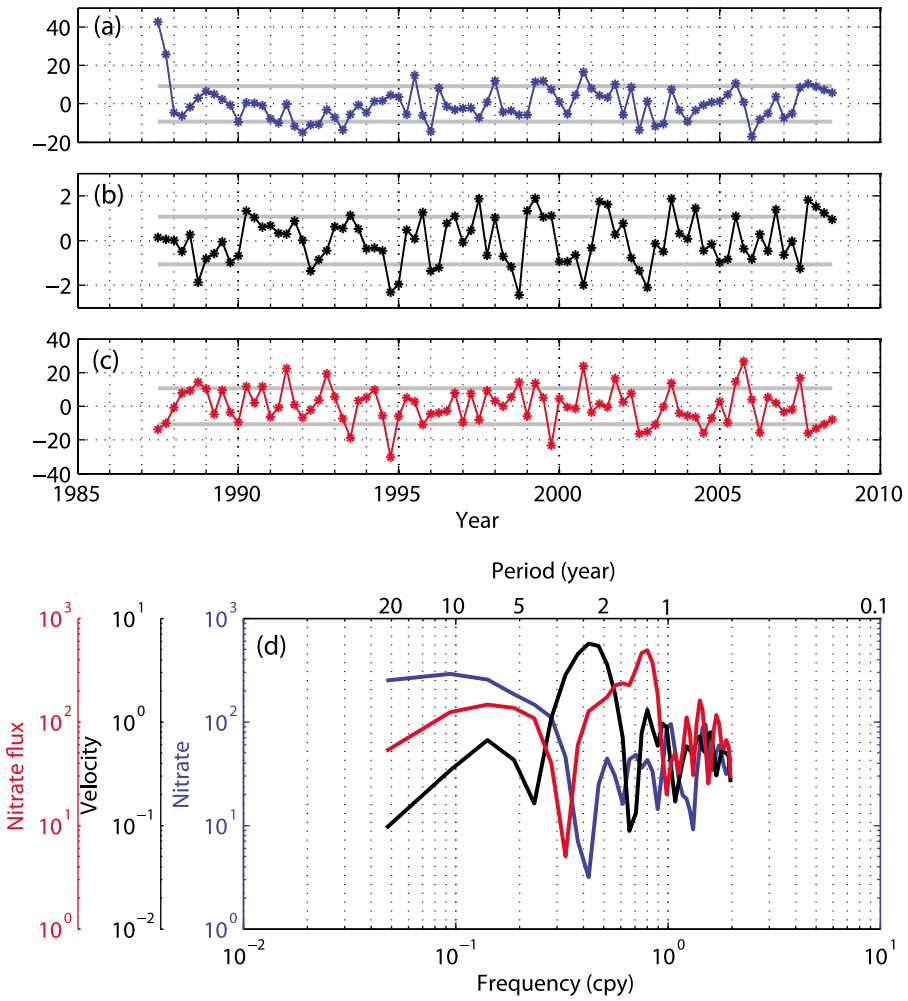

Figure 11. The same as Figure 9 but for the second EOF principal components.

The mean value of nutrient flux ($\bar{F}$) becomes

$$\bar{F} = \bar{V}\bar{C} + \frac{1}{N}\sum_{i=1}^{N} V_i' C_i'. \quad (2)$$

After introducing a new symbol $G_i = V_i' C_i'$ and substituting

$$\bar{G} = \frac{1}{N}\sum_{i=1}^{N} V_i' C_i'$$

into equation (2), we have

$$\bar{F} = \bar{V}\bar{C} + \bar{G}. \quad (3)$$

The variance of nutrient flux (σ_F^2) is defined as

$$\sigma_F^2 = \frac{1}{N}\sum_{i=1}^{N} (F_i - \bar{F})^2. \quad (4)$$

Substituting equations (1) and (3) into equation (4), we can obtain

$$\sigma_F^2 = \bar{C}^2\sigma_V^2 + \bar{V}^2\sigma_C^2 + 2\bar{C}\bar{V}\sigma_{CV}^2 + 2\bar{C}\sigma_{VG}^2 + 2\bar{V}\sigma_{CG}^2 + \sigma_G^2. \quad (5)$$

Here

$$\sigma_V^2 = \frac{1}{N}\sum_{i=1}^{N}(V_i - \bar{V})^2, \sigma_C^2 = \frac{1}{N}\sum_{i=1}^{N}(C_i - \bar{C})^2,$$

$$\sigma_{CV}^2 = \frac{1}{N}\sum_{i=1}^{N}(C_i - \bar{C})(V_i - \bar{V}),$$

$$\sigma_{VG}^2 = \frac{1}{N}\sum_{i=1}^{N}(V_i - \bar{V})(G_i - \bar{G}), \sigma_{CG}^2 = \frac{1}{N}\sum_{i=1}^{N}(C_i - \bar{C})(G_i - \bar{G}),$$

$$\sigma_G^2 = \frac{1}{N}\sum_{i=1}^{N}(G_i - \bar{G})^2.$$

According to equation (5), the variance of nutrient flux σ_F^2 is composed of six terms, in which $\bar{C}^2\sigma_V^2$ arises from mean nutrient concentration and variance of velocity; $\bar{V}^2\sigma_C^2$ from mean velocity and variance of nutrient concentration; $2\bar{C}\bar{V}\sigma_{CV}^2$ from mean velocity, mean nutrient concentration and covariance of velocity and nutrient concentration; $2\bar{C}\,\sigma_{VG}^2$ from mean nutrient concentration and covariance of velocity and G_i; $2\bar{V}\sigma_{CG}^2$ from mean velocity and covariance of nutrient concentration and G_i; σ_G^2 is variance of G_i.

[26] The left-hand side of equation (5) is presented in Figure 13a, while the six terms from the right-hand side of

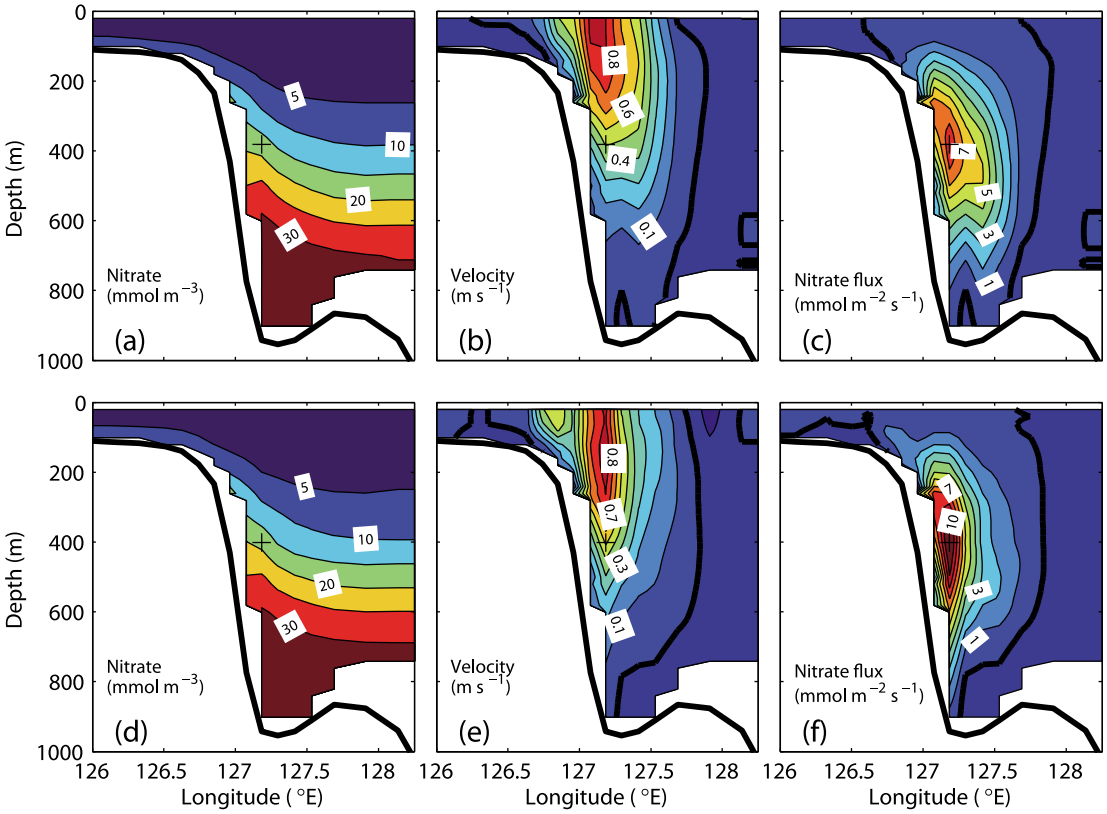

Figure 12. The same as Figure 10 but for the second EOF principal component.

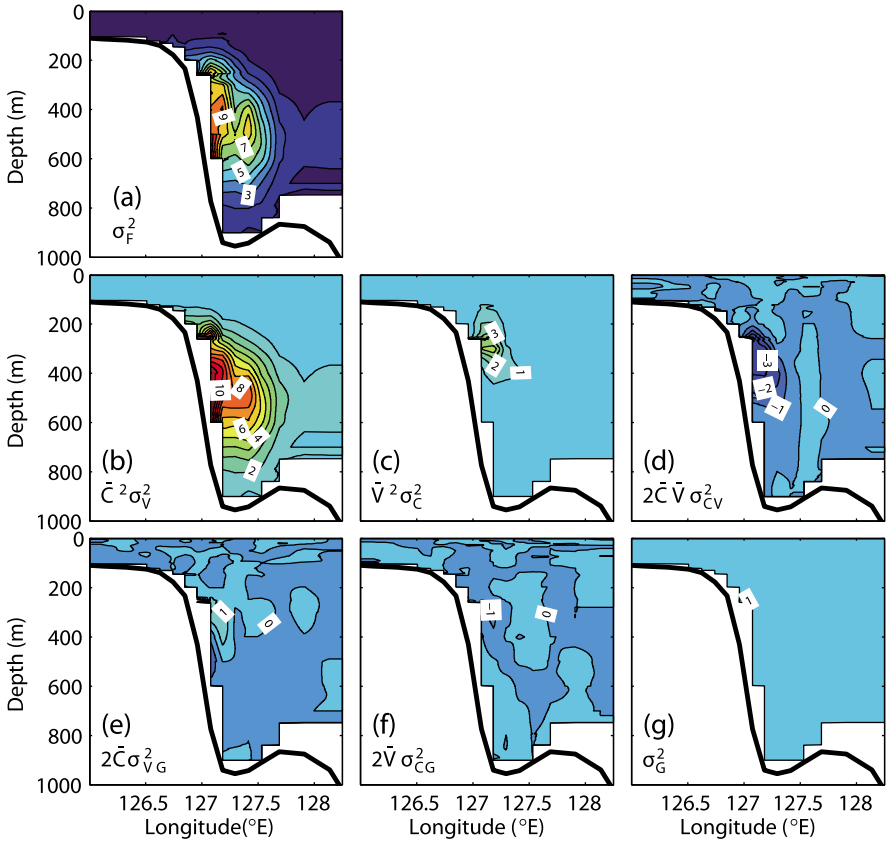

Figure 13. Total variance of nitrate (a) flux and (b–g) the six terms decomposed following equation (5).

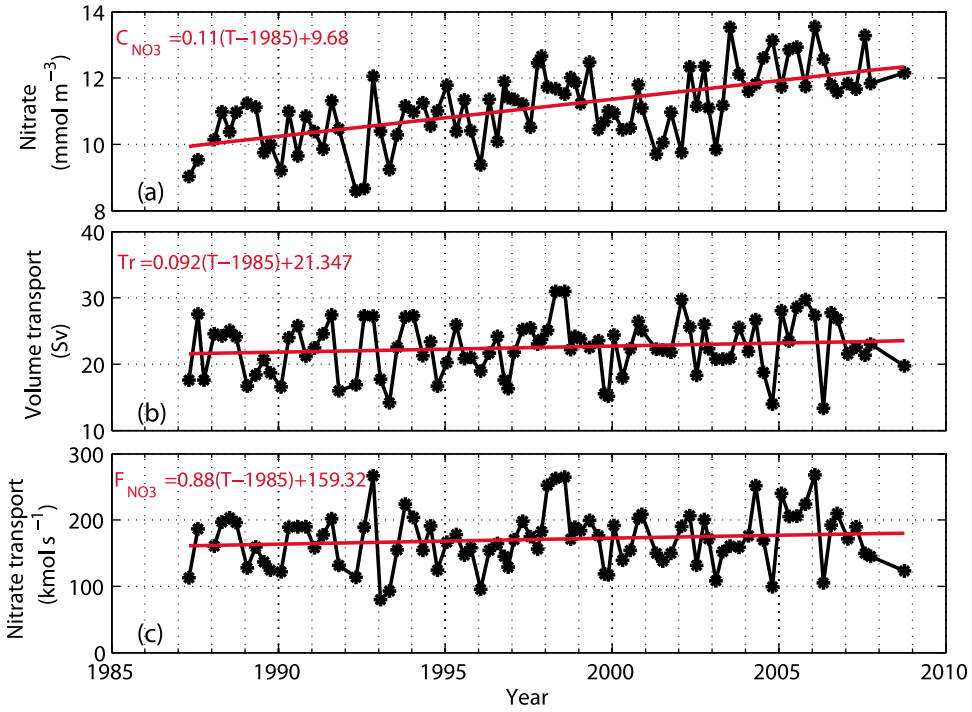

Figure 14. Time series of (a) section-averaged nitrate concentration, (b) section-integrated velocity (= volume transport), and (c) section-integrated nitrate flux (= nitrate transport). The red line in each plot denotes linear regression versus time (year).

equation (5) are in Figures 13b–13g, respectively. It is apparent that the term of $\bar{C}^2\sigma_V^2$ (Figure 13b) is the major component in variance of the nutrient flux (σ_F^2). The terms of $\bar{V}^2\sigma_C^2$ and $2\bar{C}\bar{V}\sigma_{CV}^2$ are smaller than the term of $\bar{C}^2\sigma_V^2$ but they are not small enough to be negligible. These results suggest that the temporal variation in the current velocity causes most temporal variation in the nutrient flux, while the temporal variation in the nutrient concentration and the covariance of velocity and nutrient concentration also contribute to the temporal variation in the nutrient flux.

3.4. Temporal Variations of Nutrient Transport

[27] The mean nutrient transport through section PN during the period from 1987 to 2009 is 170.8 kmol s^{-1} for nitrate (Figure 3e) and 12.7 kmol s^{-1} for phosphate (Figure 3f), respectively. The seasonal mean nitrate (phosphate) transport, which was calculated from Figure 7 or corresponding figure for phosphate (not shown here), is 172.7 (12.5) kmol s^{-1}, 177.1 (13.6) kmol s^{-1}, 161.5 (12.6) kmol s^{-1}, and 166.7 (12.8) kmol s^{-1}, for spring, summer, autumn, and winter, respectively.

[28] In the past two decades, the section-averaged nitrate concentration varied within a range between 8 and 14 mmol m^{-3} (Figure 14a) and had a standard deviation of 1.1 mmol m^{-3}. An increasing trend can be identified in Figure 14a. In particular, the section-averaged nitrate concentration was at a high level (>12 mmol m^{-3}) after 2004. The same feature may also be found in time series of the EOF1 principal component of nitrate concentration (Figure 9a).

[29] The volume transport through section PN varied between 15 and 30 Sv (Figure 14b) and had a standard deviation of 4.1 Sv. It is difficult to identify a significant increasing or decreasing trend in the volume transport, although we present the linear regression equation in Figure 14b.

[30] The nitrate transport through section PN (Figure 14c) varied within a range between ~100 and ~280 kmol s^{-1} and had a standard deviation of 41.6 kmol s^{-1}. This standard deviation actually represents an interannual variability because the standard deviation in each season, which was calculated from values in the same season but in different years, changes little: 48.7 kmol s^{-1} in spring, 44.1 kmol s^{-1} in summer, 42.3 kmol s^{-1} in autumn, and 52.2 kmol s^{-1} in winter.

[31] From Figure 14, again, we can understand the more important role of current velocity or the volume transport of the Kuroshio compared to the nitrate concentration in the temporal variation of nitrate transport. The correlation coefficient between volume transport (Figure 14b) and nitrate transport (Figure 14c) is 0.61, while that between section-averaged nitrate concentration (Figure 14a) and nitrate transport (Figure 14c) is 0.12.

[32] The result that an apparent increasing trend in section-averaged nitrate concentration (Figure 14a) does not induce an apparent increasing trend in the nitrate transport (Figure 14c) is an interesting issue. Using the linear increasing rate of three variables in Figure 14, we know that the section-averaged nitrate concentration increased by 2.2 mmol m^{-3}, the volume transport by 1.84 Sv, and the nitrate transport by 17.6 kmol s^{-1} in past 20 years. The ratio of these numbers to their corresponding values at 1985 is 0.23, 0.086, and 0.11, respectively.

[33] To understand why there is no apparent response in nitrate transport to the increasing trend in section-averaged nitrate concentration, we averaged all the data before 2004 and after 2004. We present the mean before 2004, the mean

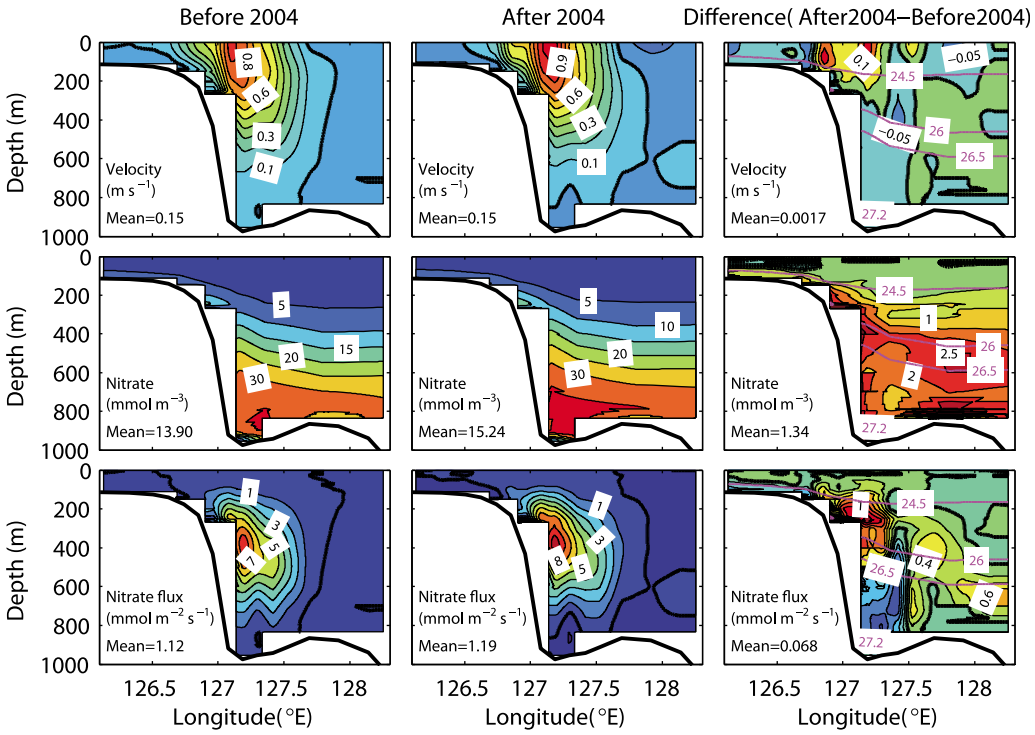

Figure 15. Velocity, nitrate concentration, and nitrate flux averaged from all the data before 2004, after 2004, and the difference (after 2004 – before 2004). The red lines with red numbers in the plots at right denote isopycnal layers.

after 2004 and their difference (before 2004 – after 2004) in Figure 15. The difference in velocity field is the intensification of the surface current and weakening of the middle and deep currents in the Kuroshio mainstream, indicating an increase in the vertical shear of current velocity, i.e., the intensification of Kuroshio baroclinicity. The increase in nitrate concentration occurred mostly in the places deeper than 200 m, with one maximum value (~2.5 mmol m^{-3}) between 400 m to 600 m depth where the water density is 26.0 ~ 26.5 σ_θ and another one (~3.0 mmol m^{-3}) at 800 m depth where the water density is around 27.0 σ_θ. The nitrate flux shows a positive difference above 500 m depth but a negative difference below it. Since the positive and negative nitrate flux differences canceled each other, the increase in nitrate transport through the section is small.

4. Discussions

4.1. Causes for Differences in Velocity and Nutrients Before 2004 and After 2004

[34] The variations in velocity field (Figure 15) have close relation to the difference in water temperature and salinity before 2004 and after 2004 (Figure 16). In the surface layer, the water temperature increased while the salinity decreased. Both of them induced a reduction in surface density. An important point is that the magnitude of difference in surface water temperature and salinity varied horizontally. The water temperature (salinity) increased (decreased) more at offshore side of Kuroshio than at its mainstream. Consequently, the horizontal gradient of surface density increased. The increased horizontal density gradient then intensified vertical shear of the velocity according to thermal wind relation of a geostrophic current.

[35] The causes for nutrient increases in the middle layer (26.0–26.5 σ_θ) and bottom layer (~27.0 σ_θ) (Figure 15) are more complex. The nitrate increase in the middle layer was accompanied by apparent reduction in water temperature, salinity, and dissolved oxygen (Figure 16). However, the nitrate increase in the bottom layer was accompanied by an increase in water temperature, salinity and dissolved oxygen (Figure 16). Therefore, it is reasonable to separate the causes for nutrient increase in two layers.

[36] The change in water mass property of the central mode water with a core density of 26.2 σ_θ [*Nakano et al.*, 2007; *Kouketsu et al.*, 2009] is the first possible cause responsible for the nitrate increase at section PN after 2004, in particular for that in the middle layer (26.0–26.5 σ_θ). *Nakano et al.* [2007] reported freshening at mid-depth (between the main thermocline and salinity minimum layer of NPIW) in the North Pacific subtropical gyre and attributed it to the isopycnal surface deepening due to subsurface water warming, and to westward shifts of the salinity minimum tongue due to strengthening of the subtropical gyre. *Kouketsu et al.* [2009] confirmed the freshening and warming effects and additionally reported increase in apparent oxygen utilization and silicate around the density of central mode water. Although we do not have silicate data, we can identify declines in water temperature, salinity, dissolved oxygen and increase in nitrate for the water with density 26.0 ~ 26.5 σ_θ after 2004 in Figure 16. All these features are consistent with those reported by *Nakano et al.* [2007] and *Kouketsu et al.* [2009].

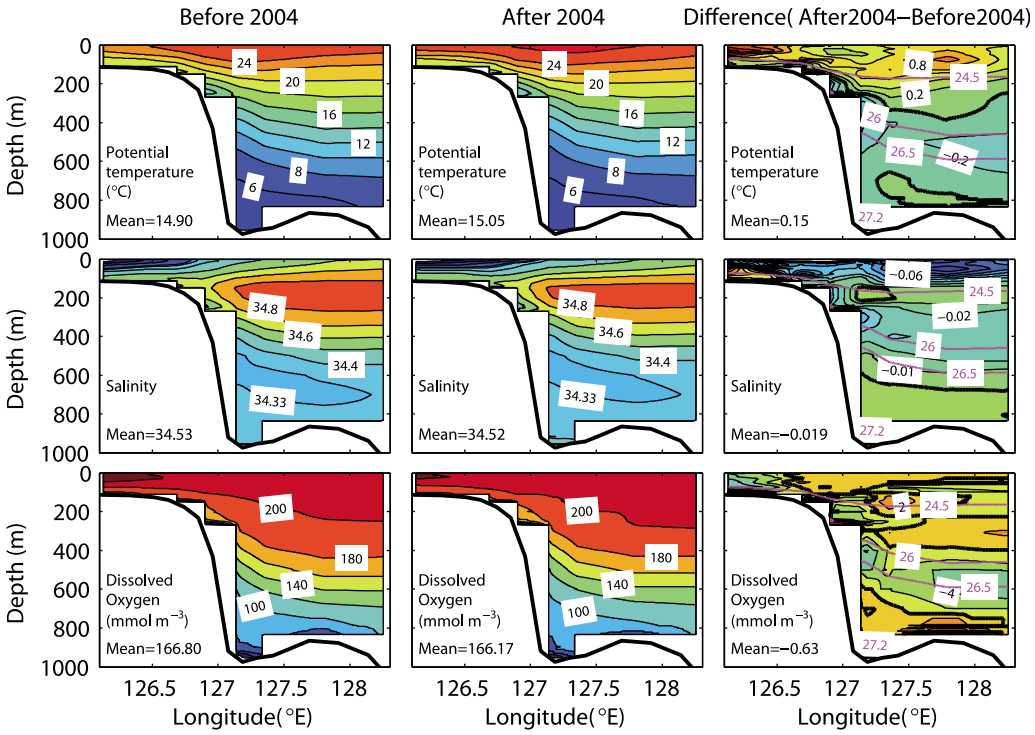

Figure 16. Potential temperature, salinity, and dissolved oxygen averaged from all the data before 2004, after 2004, and the difference (after 2004 – before 2004). The red lines with red numbers in each plot at right denote isopycnal layers.

[37] The second possible cause responsible for the nitrate increase at section PN after 2004 is the temporal changes in formation regions of NPIW [*Ono et al.*, 2001; *Watanabe et al.*, 2001; *Nakanowatari et al.*, 2007; *Watanabe et al.*, 2008]. As estimated by *You et al.* [2003], the westward transport of NPIW across a section at 130°E is 3.9 Sv, a part of which is expected to enter the South China Sea via the Luzon Strait [*You*, 2003], a strait between Taiwan and Luzon Island (Figure 1a), and eventually return to the Kuroshio region by the outflow of South China Sea intermediate water [*Chen*, 2005]. The change in NPIW should affect more the nitrate increase in the bottom layer than in the middle layer after 2004 because the middle layer is above the salinity minimum at section PN (Figure 16). The fact that the minimum salinity is higher at section PN than in the NPIW in the subtropical gyre indicates that the mixing of NPIW with other water masses may weaken the interannual signals of NPIW in its formation regions as they reach at section PN.

[38] The third possible cause responsible for the nitrate increase at section PN after 2004 is the outflow of nutrient-rich South China Sea intermediate water to the Kuroshio region through the Luzon Strait [*Chen and Huang*, 1996; *Chen and Wang*, 1998; *Chen*, 2005; *Chou et al.*, 2007]. The changes in the volume transport or in the water property of South China Sea intermediate water can induce an increase or decrease in nutrient concentrations at section PN, in particular at western side of Kuroshio mainstream. The fourth possible cause is the intensification of Kuroshio baroclinicity since the interaction between bathymetry and Kuroshio baroclinicity affects the water movement across the shelf break [*Guo et al.*, 2006].

[39] In Figure 17, we present the time series of water temperature, salinity, nitrate, dissolved oxygen, velocity, and nitrate flux in three isopycnal layers (24.5–26.0 σ_θ, 26–26.5 σ_θ, 26.5–27.2 σ_θ) for understanding the realizations behind the "state" change after 2004 (Figures 15 and 16). We neglect the surface and bottom layers because they contribute little to nutrient transport through the section (Figure 6b).

[40] The temporal variations in Figure 17 can be divided into two parts: linear trend and interannual variations. According to the linear regression equations in each panel of Figure 17, the trends of water temperature, salinity, velocity, and nitrate flux in three layers are not as apparent as nitrate concentration and dissolved oxygen. Qualitatively, the two apparent trends of nitrate concentration and dissolved oxygen have an inverse relation in three isopycnal layers, indicating important role of microbial respiration. Quantitatively, the ratio of increasing rate of nitrate concentration and decreasing rate of dissolved oxygen changes largely in three layers. The increasing rates of nitrate concentration in three layers are of the same order, but the decreasing rates of dissolved oxygen in three layers are of different order. Therefore, in addition to the microbial respiration, the water property changes in mode waters [*Nakano et al.*, 2007; *Kouketsu et al.*, 2009] and the linear trends in the NPIW [*Ono et al.*, 2001; *Watanabe et al.*, 2001; *Nakanowatari et al.*, 2007; *Watanabe et al.*, 2008] are also important factors affecting the linear trend. Additional evidence for supporting this deduction is that there is no apparent trend of weakening in the velocity in three layers.

[41] The interannual variations, as presented by one year running mean in Figure 17, have a time scale of several

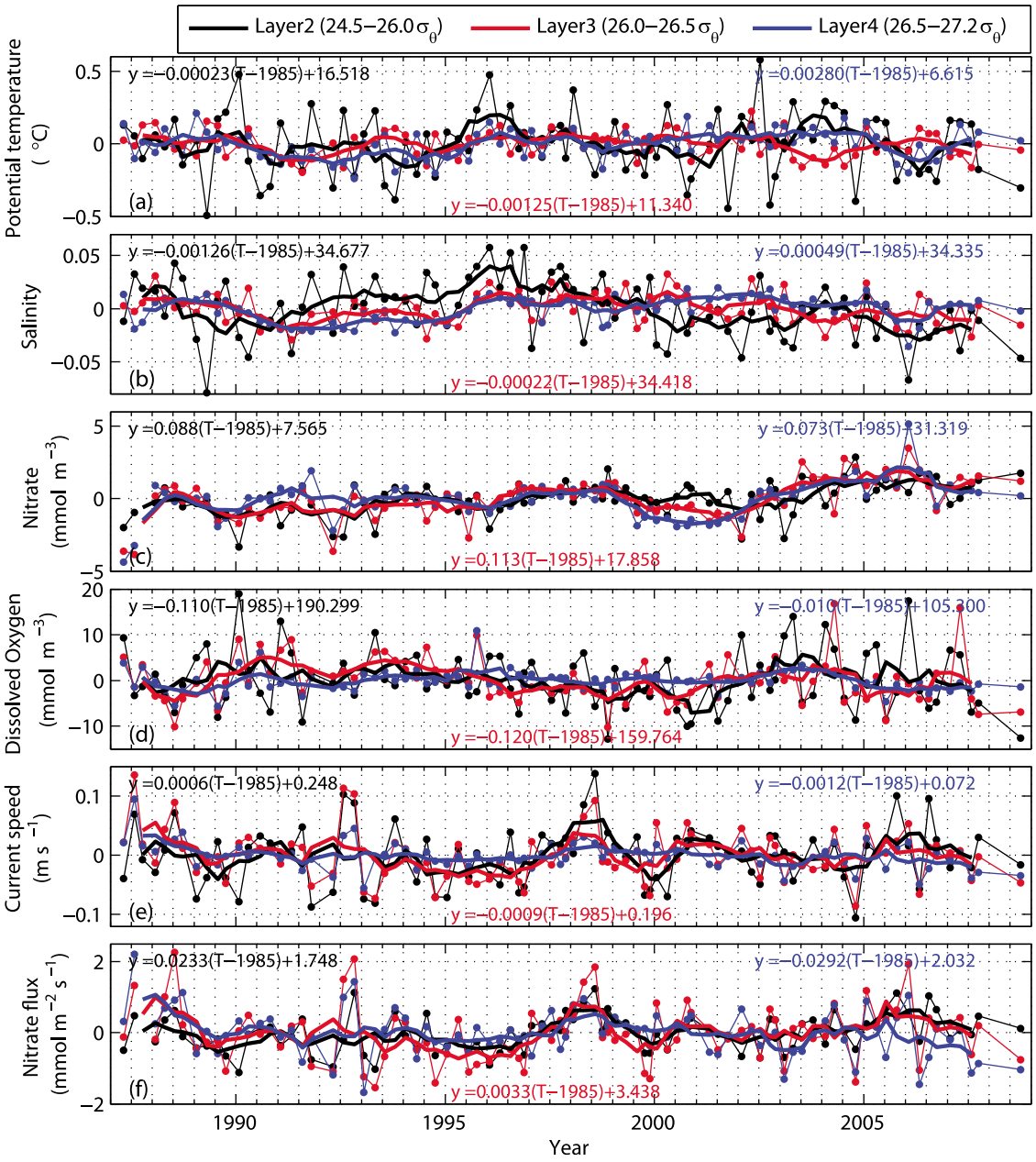

Figure 17. Anomalies (thin lines with dots) and their 1 year running means (bold lines) of (a) potential temperature, (b) salinity, (c) nitrate concentration, (d) dissolved oxygen, (e) current velocity, and (f) nitrate flux averaged in three isopycnal layers (24.5–26.0 σ_θ, 26.0–26.5 σ_θ, and 26.5–27.2 σ_θ). The anomalies were obtained by removing mean value over the entire observation period from raw data. The linear regression equation was calculated from raw data. In all plots, black color denotes variables from layer 2 (24.5–26.0 σ_θ), red color from layer 3 (26.0–26.5 σ_θ), and blue color from layer 4 (26.5–27.2 σ_θ).

years. Due to short length of time series, we cannot identify a significant period for interannual variations by using energy spectra analysis and wavelet analysis. Nevertheless, the realizations of high nitrate concentration level after 2004 becomes clear. The overlap of a positive phase of interannual variations and the linear increasing trend is its direct reason. The interannual variations induced not only the period with high level of nutrient concentration (1997–1999; 2004–2006) but also that with low level of nutrient concentration (2000–2002). Among three layers, the layer of 26.5–27.2 has the largest range of interannual variations in nitrate concentration (Figure 17c) but smallest range of interannual variations in dissolved oxygen and in velocity (Figure 17d).

[42] The interannual variations of nitrate concentration and dissolved oxygen do not match in phase (Figure 17). The peak (trough) of dissolved oxygen is generally later than the trough (peak) of nitrate concentration by several years. This mismatch of phase suggests again that microbial respiration is not the sole process controlling the interannual variations of two variables at section PN.

4.2. Comparisons With Nutrient Flux and Nutrient Transport by the Kuroshio East of Taiwan and by the Gulf Stream

[43] A comparison of nutrient flux at section PN (Figure 3) to previously reported results at different places is helpful to understand the factors controlling spatial structure of nutrient flux. *Chen et al.* [1994] reported a maximum core at 500 m depth in the phosphate flux (there is no nitrate flux in this paper) through a section east of Taiwan, which is located upstream of the Kuroshio relative to section PN. Comparing this with our results (Figure 3f), we know that the depth of maximum nutrient flux was lifted upward by 100 m as the Kuroshio moves from the section east of Taiwan to section PN. The maximum value of the phosphate flux reported by *Chen et al.* [1994] is $\sim$0.3 mmol m^{-2} s^{-1}, or half of our maximum value $\sim$0.6 mmol m^{-2} s^{-1}. This is mainly due to the difference in velocity at the depth of maximum core of nutrient flux: $\sim$0.2 m s^{-1} in the work by *Chen et al.* [1994] but $\sim$0.4 m s^{-1} in this study.

[44] Although the maximum value of the phosphate flux is smaller at the section east of Taiwan than at section PN, the phosphate transport is larger at the section east of Taiwan (22.1 kmol s^{-1}) than at section PN (12.7 kmol s^{-1}). The current structure is likely the main cause for such difference. Two cores of strong northward current can be found at the section east of Taiwan of *Chen et al.* [1994] but the offshore core is not a part of the Kuroshio. As reported by *Chen et al.* [1995a] and also in our results (Figure 14), the large temporal variability in nutrient transport makes it difficult to compare our mean state results with the results from a single "snapshot" cruise [*Chen et al.*, 1994, 1995a]. Nevertheless, the consistent spatial structure of the nutrient flux and the same order of nutrient transport suggest the presence of a nutrient stream in the Kuroshio region in the East China Sea.

[45] The nutrient flux of the Gulf Stream through a section near 36°N [*Pelegrí and Csanady*, 1991] has a maximum core at 500 m depth and a maximum value of 15 mmol m^{-2} s^{-1} for nitrate and of 0.8 mmol m^{-2} s^{-1} for phosphate, respectively. The nutrient transport was $\sim$860 kmol s^{-1} for nitrate and $\sim$55 kmol s^{-1} for phosphate, both of which are 4 $\sim$ 5 times larger than the values obtained for the Kuroshio in the East China Sea. The large nutrient flux and nutrient transport resulted from the strong currents and large volume transport in the Gulf Stream. The current speed of the Gulf Stream at the section near 36°N of *Pelegrí and Csanady* [1991] was 1.4 m s^{-1} at the surface, 0.8 m s^{-1} at 500 m depth, and 0.2 m s^{-1} at 900 m depth. The corresponding current speed of the Kuroshio at section PN is $\sim$0.8 m s^{-1}, $\sim$0.4 m s^{-1} and 0 m s^{-1}, respectively. Clearly, the Gulf Stream is stronger than the Kuroshio and must transport more water and nutrients. However, this is not the sole cause. The volume transport between the Gulf Stream near 36°N and the Kuroshio at section PN is 3 times greater, but the nutrient transport is 4–5 times greater. Therefore, the higher nutrient concentration carried by the Gulf Stream compared to the Kuroshio is another important cause. For example, the nitrate concentration around the maximum nitrate flux at 500 m depth in the Gulf Stream ranged from 20 to 25 mmol m^{-3}, but the concentration around the maximum nitrate flux at 400 m depth in the Kuroshio ranged from 10 to 20 mmol m^{-3}. Since the nutrient concentration generally increases with depth in both the Gulf Stream and Kuroshio, the deeper current structure of the Gulf Stream compared to the Kuroshio could be the direct cause of the larger nutrient flux in the Gulf Stream.

5. Conclusions

[46] In this study, we not only presented the mean state of nutrient flux by the Kuroshio calculated from 88 data sets from 1987 to 2009 in the East China Sea, but also examined its temporal variations. The seasonal variation in the nutrient flux is slight and much smaller than the interannual variation. EOF analysis of the nitrate concentration, velocity field, and nutrient flux suggested that the changes in the Kuroshio speed and current structure are the major causes for interannual variation in the nutrient flux. This conclusion is further confirmed by directly decomposing the variance of nutrient flux into terms depending on the variances of nutrient concentration and velocity.

[47] The downstream nitrate transport by the Kuroshio has a mean value of 170.8 kmol s^{-1} and a standard deviation of 41.6 kmol s^{-1}. Its mean seasonal variation ranges from 161.5 to 177.1 kmol s^{-1} and its absolute interannual variation ranges from about 100 to 280 kmol s^{-1}.The mean onshore nutrient transport from the Kuroshio to the continental shelf of the East China Sea was estimated to be 9.4 kmol s^{-1} for the nitrate and 0.7 kmol s^{-1} for the phosphate [*Zhao and Guo*, 2011], both of which are 1/18 of the downstream nutrient transport by the Kuroshio. Consequently, the nutrients within the nutrient stream of the Kuroshio are essentially transported downstream toward the south of Japan and Kuroshio Extension area.

[48] The nitrate concentration at section PN, especially in the middle and deep layers, increased significantly after 2004, but the nutrient transport did not increase significantly. The small change in nutrient transport can be explained by the fact that the velocity increased in the surface layer but decreased in the middle and bottom layers after 2004. The direct cause for intensification of vertical shear in the Kuroshio is the warming and freshening of surface layer after 2004 that had a larger magnitude at the offshore side. The direct cause for nutrient increase in the middle and bottom layers is the overlap of linear increasing trend and positive phase of interannual variations of nutrient concentration. Four possible causes are (1) water property changes of subtropical mode waters in the North Pacific, (2) changes in formation of NPIW, (3) changes in outflow of South China Sea Intermediate Water toward the Kuroshio region, and (4) dynamic response of water movement across the shelf break of the East China Sea to the intensification of Kuroshio baroclinicity, were suggested to be responsible for the observed variations in nutrient concentrations in the middle and bottom layers.

[49] **Acknowledgments.** This study is supported by JSPS KAKENHI (21310012) and by multiple sponsors on the Chinese side: (1) the National Natural Science Foundation of China (41176021, 40776021), (2) the National Basic Research Program of China (2011CB409803, 2011CB403503), (3) the Young Ocean Foundation of the SOA (2010229), (4) Overseas, Hong Kong and Macao Scholars Collaborated Researching Fund from National Science Foundation of China (41028006), and (5) the Open Fund of Key Laboratory of Marine Ecosystem and Biogeochemistry, SOA (LMEB201107). Comments from J. L. Pelegrí and two anonymous reviewers were helpful in improving the original manuscript.

References

Aoyama, M., et al. (2008), Marine biogeochemical response to a rapid warming in the main stream of the Kuroshio in the western North Pacific, *Fish. Oceanogr.*, *17*, 206–218, doi:10.1111/j.1365-2419.2008.00473.x.

Chen, C. T. A. (2005), Tracing tropical and intermediate waters from the South China Sea to the Okinawa Trough and beyond, *J. Geophys. Res.*, *110*, C05012, doi:10.1029/2004JC002494.

Chen, C. T. A., and M. H. Huang (1996), A mid-depth front separating the South China Sea water and the west Philippine Sea water, *J. Oceanogr.*, *52*, 17–25, doi:10.1007/BF02236530.

Chen, C. T. A., and S. L. Wang (1998), Influence of intermediate water in the western Okinawa Trough by the outflow from the South China Sea, *J. Geophys. Res.*, *103*, 12,683–12,688, doi:10.1029/98JC00366.

Chen, C. T. A., C. T. Liu, and S. C. Pai (1994), Transport of oxygen, nutrients and carbonates by the Kuroshio Current, *Chin. J. Oceanology Limnol.*, *12*, 220–227, doi:10.1007/BF02845167.

Chen, C. T. A., C. T. Liu, and S. C. Pai (1995a), Variations in oxygen, nutrient and carbonate fluxes of the Kuroshio Current, *Mer*, *33*, 161–176.

Chen, C. T. A., R. Ruo, S. C. Pai, C. T. Liu, and G. T. F. Wong (1995b), Exchange of water masses between the East China Sea and the Kuroshio off northeastern Taiwan, *Cont. Shelf Res.*, *15*, 19–39, doi:10.1016/0278-4343(93)E0001-O.

Chou, W. C., D. D. Sheu, C. T. A. Chen, L. S. Wen, Y. Yang, and C. L. Wei (2007), Transport of the South China Sea subsurface water outflow and its influence on carbon chemistry of Kuroshio waters off southeastern Taiwan, *J. Geophys. Res.*, *112*, C12008, doi:10.1029/2007JC004087.

Guo, X., H. Hukuda, Y. Miyazawa, and T. Yamagata (2003), A triply nested ocean model for simulating the Kuroshio—Roles of horizontal resolution on JEBAR, *J. Phys. Oceanogr.*, *33*, 146–169, doi:10.1175/1520-0485(2003)033<0146:ATNOMF>2.0.CO;2.

Guo, X., Y. Miyazawa, and T. Yamagata (2006), The Kuroshio onshore intrusion along the shelf break of the East China Sea: The origin of the Tsushima Warm Current, *J. Phys. Oceanogr.*, *36*, 2205–2231, doi:10.1175/JPO2976.1.

Hinata, T. (1996), Seasonal variation and long-term trends of the oceanographic conditions along a fixed hydrographic line crossing the Kuroshio in the East China Sea, *Oceanogr. Mag.*, *45*, 9–32.

Kouketsu, S., M. Fukasawa, I. Kaneko, T. Kawano, H. Uchida, T. Doi, M. Aoyama, and K. Murakami (2009), Changes in water properties and transports along 24°N in the North Pacific between 1985 and 2005, *J. Geophys. Res.*, *114*, C01008, doi:10.1029/2008JC004778.

Nakano, T., I. Kaneko, T. Soga, H. Tsujino, T. Yasuda, H. Ishizaki, and M. Kamachi (2007), Middepth freshening in the North Pacific subtropical gyre observed along the JMA repeat and WOCE hydrographic sections, *Geophys. Res. Lett.*, *34*, L23608, doi:10.1029/2007GL031433.

Nakanowatari, T., K. I. Ohshima, and M. Wakatsuchi (2007), Warming and oxygen decrease of intermediate water in the northwestern North Pacific, originating from the Sea of Okhotsk, 1955–2004, *Geophys. Res. Lett.*, *34*, L04602, doi:10.1029/2006GL028243.

Oka, E., and M. Kawabe (1998), Characteristics of variations of water properties and density structure around the Kuroshio in the East China Sea, *J. Oceanogr.*, *54*, 605–617, doi:10.1007/BF02823281.

Ono, T., T. Midorikawa, Y. W. Watanabe, K. Tadokoro, and T. Saino (2001), Temporal increases of phosphate and apparent oxygen utilization in the subsurface waters of western subarctic Pacific from 1968 to 1998, *Geophys. Res. Lett.*, *28*(17), 3285–3288, doi:10.1029/2001GL012948.

Pelegrí, J. L., and G. T. Csanady (1991), Nutrient transport and mixing in the Gulf Stream, *J. Geophys. Res.*, *96*, 2577–2583, doi:10.1029/90JC02535.

Pelegrí, J. L., G. T. Csanady, and A. Martins (1996), The North Atlantic nutrient stream, *J. Oceanogr.*, *52*, 275–299, doi:10.1007/BF02235924.

Pelegrí, J. L., A. Marrero-Diaz, and A. W. Ratsimandresey (2006), Nutrient irrigation in the North Atlantic, *Prog. Oceanogr.*, *70*, 366–406, doi:10.1016/j.pocean.2006.03.018.

Robbins, P. E., and H. L. Bryden (1994), Direct observations of advective nutrient and oxygen fluxes at 24°N in the Pacific Ocean, *Deep Sea Res., Part I*, *41*, 143–168, doi:10.1016/0967-0637(94)90030-2.

Tadokoro, K., T. Ono, I. Yasuda, S. Osafune, A. Shiomoto, and H. Sugisaki (2009), Possible mechanisms of decadal-scale variation in PO4 concentration in the western North Pacific, *Geophys. Res. Lett.*, *36*, L08606, doi:10.1029/2009GL037327.

Watanabe, Y. W., T. Ono, A. Shimamoto, T. Sugimoto, M. Wakita, and S. Watanabe (2001), Probability of a reduction in the formation rate of the subsurface water in the North Pacific during the 1980s and 1990s, *Geophys. Res. Lett.*, *28*(17), 3289–3292, doi:10.1029/2001GL013212.

Watanabe, Y. W., M. Shigemitsu, and K. Tadokoro (2008), Evidence of a change in oceanic fixed nitrogen with decadal climate change in the North Pacific subpolar region, *Geophys. Res. Lett.*, *35*, L01602, doi:10.1029/2007GL032188.

Williams, R. G., V. Roussenov, and M. J. Follows (2006), Nutrient streams and their induction into the mixed layer, *Global Biogeochem. Cycles*, *20*, GB1016, doi:10.1029/2005GB002586.

Wunsch, C. (1978), The North Atlantic general circulation west of 50°W determined by inverse methods, *Rev. Geophys.*, *16*, 583–620, doi:10.1029/RG016i004p00583.

You, Y. (2003), The pathway and circulation of North Pacific Intermediate Water, *Geophys. Res. Lett.*, *30*(24), 2291, doi:10.1029/2003GL018561.

You, Y., N. Suginohara, M. Fukasawa, H. Yoritaka, K. Mizuno, Y. Kashino, and D. Hartoyo (2003), Transport of North Pacific Intermediate Water across Japanese WOCE sections, *J. Geophys. Res.*, *108*(C6), 3196, doi:10.1029/2002JC001662.

Zhao, L., and X. Guo (2011), Influence of cross-shelf water transport on nutrients and phytoplankton in the East China Sea: A model study, *Ocean Sci.*, *7*, 27–43, doi:10.5194/os-7-27-2011.

Zhu, X.-H., J.-H. Park, and I. Kaneko (2006), Velocity structures and transports of the Kuroshio and the Ryukyu Current during fall of 2000 estimated by an inverse technique, *J. Oceanogr.*, *62*, 587–596, doi:10.1007/s10872-006-0078-y.

X. Guo, Center for Marine Environmental Studies, Ehime University, 2-5 Bunkyo-cho, Matsuyama 790-8577, Japan. (guoxinyu@sci.ehime-u.ac.jp)

D. Huang, Q.-S. Wu, and X.-H. Zhu, State Key Laboratory of Satellite Ocean Environment Dynamics, Second Institute of Oceanography, State Oceanic Administration, Hangzhou 310012, China.